What Controls the Amplitude and Phase of the Extratropical Seasonal Cycle?

Alex Hall*, Ronald J. Stouffer, Richard T. Wetherald,****

Kuo-Nan Liou*, and Cynthia Shih*

*Department of Atmospheric Sciences

University of California, Los Angeles

Los Angeles, California

**Geophysical Fluid Dynamics Laboratory

Princeton, New Jersey

corresponding author address:

Prof. Alex Hall

Department of Atmospheric Sciences

*University of California, Los Angeles

Los Angeles, CA 90095

e-mail: alexhall@atmos.ucla.edu

submitted to *Journal of Climate*

Abstract

The seasonal cycle of mid to high latitude surface air temperature is prime example of a climate response to external forcing. Here we examine what controls the amplitude and phase of this cycle. By comparing the seasonal cycle in an numerical model of the atmosphere and ocean mixed layer where the large seasonal variation in humidity is allowed to affect longwave radiation to one where it is not, we examine the impact of water vapor feedback on seasonal cycle amplitude and phase. Water vapor feedback is thought to be the most powerful positive feedback to climate variations. However, it has a surprisingly small amplifying affect of about 10-20% on the overall amplitude of the extratropical seasonal cycle. Its effect on phase is also small. This is mainly because the extratropical seasonal cycle is damped not only by radiative processes, but also by heat exchange between the extratropics and tropics. When temperatures are cold (warm) during winter (summer), an anomalously large (small) amount of heat is transported from the tropics into the extratropics. On a Wm^{-2} basis, this damping mechanism is slightly more effective than radiative damping, substantially diluting the effects of the classical radiative climate feedbacks such as water vapor feedback. Because the seasonal cycle is so effectively damped by both radiative fluxes and horizontal heat exchange, it is in equilibrium with the solar forcing to a surprisingly large degree, with a much smaller amplitude than would be expected if radiative feedbacks alone were responsible for the damping. We also show that if there were no lateral damping, the amplitude of the mid to high latitude seasonal cycle would increase by approximately 50% in both hemispheres, while its lag behind the solar forcing would increase from one to about two months.

1 Climate Sensitivity and the Seasonal Cycle

The controls on the sensitivity of the atmosphere-ocean system to thermal forcing is a major focus of current climate research. In particular, many have focused on the role of radiative feedbacks, such as water vapor feedback (Hall and Manabe 1999, Held and Soden 2000), cloud feedback (Hartmann and Larson 2002, Lindzen et al. 2001, Cess et al. 1996, Mitchell and Ingram, 1992, Wetherald and Manabe, 1988), and surface albedo feedback (Hall 2003, Cess et al. 1991, Ingram et al. 1989, Robock 1983, Manabe and Wetherald 1980), in shaping the climate response to anthropogenic forcing such as an increase in greenhouse gases. Others have noted the role of radiative feedbacks in the climate response to natural forcings, such as the presence of large ice sheets at high latitudes of the northern hemisphere (NH) and the simultaneous lowering of CO_2 at the last glacial maximum (e.g. Broccoli 2000).

Though the present-day seasonal cycle of surface air temperature (SAT) in mid to high latitudes is also a prime example of externally-forced climate variability, it is usually taken somewhat for granted, viewed as an element of the climate system's mean state, rather than as an object of curiosity in its own right. Yet the relationship between the seasonal cycle of solar forcing and the SAT response to it is not understood beyond the obvious observation that it is warmer when there is more sunshine in the summer, and cooler when there is less in the winter. Given the amplitude of the seasonal cycle of sunshine, what exactly determines the amplitude of the seasonal cycle of SAT? And given the timing of the seasonal solar forcing, what determines the phase lag of the SAT response? These climate sensitivity questions are fundamental and unresolved.

An obvious starting point for thinking about what determines the amplitude and phase of the seasonal cycle are the damping mechanisms thought to affect the amplitude and characteristic time scale of the SAT response to external forcing. The more powerful the damping, the smaller the amplitude of the seasonal cycle. Powerfully damped systems also tend to equilibrate more

quickly with external forcings, and so for quasi-sinusoidal forcings such as the seasonal cycle of sunshine, will tend to lag the forcing less.

Classical radiative climate feedbacks such as water vapor feedback can influence strongly the damping of SAT, and therefore might play a large role in determining the amplitude and phase of the seasonal cycle. Fig 1 shows the composite seasonal variation of humidity and temperature averaged over the extratropical troposphere below 300hPa. Results are shown from both hemispheres for the control climate model used in this study (see section 2 for a description of this model) and the NCEP re-analysis. In both hemispheres in model and observation, the seasonal cycle of mid to lower tropospheric humidity is quite large and is clearly tightly in phase with the seasonal variation in temperature. DelGenio et al. (1994) documented that this is also the case for upper tropospheric humidity. This is unambiguous evidence of a strongly positive water vapor feedback operating on seasonal time scales.

A starting point for this study is assessing how much classic radiative climate feedbacks affect the SAT seasonal cycle. This is done by examining explicitly the impact of water vapor feedback on the amplitude and phase of the SAT seasonal cycle in a numerical model of the atmosphere coupled to a slab mixed layer model of the ocean. The impact of water vapor feedback is isolated by prescribing humidity to annual mean values in the longwave portion of the model's radiative transfer subroutine. The resulting seasonal cycle is compared to a model where information about the seasonal variation of water vapor is passed to the model's radiation code. (See section 2 for details about the design of these experiments.)

It turns out that the large seasonal variation in water vapor portrayed in fig 1 has surprisingly little impact on the simulated amplitude and phase of the SAT seasonal cycle. To aid in understanding why this is the case, as well the mechanisms exerting greater control than the classical radiative feedbacks such as water vapor feedback on the characteristics of the seasonal cycle,

we develop a very simple conceptual framework for the SAT response to seasonal solar forcing in section 3. We can then easily manipulate this heuristic model to quantify the importance of the mechanisms it includes.

One difficulty in conceptualizing the SAT response to the seasonal variation of sunshine lies in the treatment of the forcing itself. Unlike other commonly studied thermal forcings such as an increase in CO_2, the spatial structure of the seasonal solar forcing is not globally uniform. Poleward of the Tropics of Cancer and Capricorn (23.5° latitude), the solar forcing is quasi-sinusoidal with a period of one year. This spatial structure suggests a conceptual division of the planet into three zones: A NH extratropical region bounded by 23.5°N, a southern hemisphere (SH) extratropical region bounded by 23.5°S, and a tropical zone in between. Within these two extratropical regions, the spatial structure of the forcing is quite coherent, with the timing of the maxima and minima being the same everywhere. Equatorward of 23.5° latitude the forcing has higher frequency variations and is not spatially coherent. It makes a complicated transition from a quasi-sinusoidal one-year period wave peaking on June 21 at 23.5°N, to a quasi-sinusoidal one-year period wave peaking at Dec 21 at 23.5°S. This transition introduces higher frequencies into the forcing in the tropical zone. For example, at the equator, the forcing period is six months, with maxima occurring at the two equinoxes. Because of the spatial coherence of the seasonal forcing poleward of 23.5°, we focus on the SAT response in NH and SH extratropical regions bounded by 23.5°.

Throughout most of this study, we examine the seasonal variations in climate quantities averaged over the NH and SH regions bounded by 23.5° latitude. This affords an understanding of the essential mechanisms controlling the gross characteristics of the SAT seasonal cycle in mid to high latitudes. In section 4, we present the numerical experiment results showing the effect of water vapor feedback on the seasonal variation of SAT averaged over the NH and SH regions.

We also quantify the contributions of the mechanisms contained in the heuristic model to the simulated energy budget averaged over these regions. Then, in section 5, we test the heuristic model to see whether it predicts accurately the NH and SH seasonal cycles in the numerical models with and without water vapor feedback. Once we establish that the heuristic model is formulated properly, we manipulate it to quantify the importance of the individual mechanisms it contains, thereby explaining why water vapor feedback has such a small impact on seasonal cycle amplitude and phase. In section 6, we move beyond the perspective of the SAT seasonal cycle averaged over NH and SH regions bounded by 23.5° to examine the controls on local variations of SAT seasonal cycle amplitude and phase in these regions. Finally, we summarize and discuss our results in section 7.

2 Model Description and Experimental Technique

A detailed description of the numerical model used in the experiments isolating the impact of water vapor feedback on the SAT seasonal cycle is provided in Wetherald (1996). Here we provide a brief summary. The model consists of a general circulation model of the atmosphere coupled to a simple land surface model and a thermodynamic slab model of the ocean mixed layer. The atmospheric model is global in scope. The horizontal distributions of predicted atmospheric variables are represented by spherical harmonics (30 associated Legendre functions for each of 30 Fourier components) and by grid-point values (Gordon and Stern 1982). This translates into a horizontal resolution of approximately 2.25° latitude by 3.75° longitude. The atmospheric model has 14 vertical finite difference levels. Cloud cover is predicted based on relative humidity. Insolation varies seasonally, but not diurnally. The radiative transfer model simulates the interaction of solar and terrestrial radiation with cloud, water vapor, CO_2, ozone, and the surface. The land surface model computes moisture and snow budgets, as well as surface water fluxes. Surface

heat fluxes are also calculated, with the constraint that no heat storage is allowed in the land (Manabe, 1969). The ocean mixed layer model consists of a vertically isothermal layer of water with a uniform depth of 50 m. In ice-free regions, the mixed layer temperature is computed from the net balance of the heat fluxes at the ocean surface. In ice-covered regions, the mixed layer temperature is fixed at the freezing point and the heat conduction through the ice is balanced by freezing or melting at the bottom of the ice layer. This process, together with surface melting, sublimation, and snowfall determines the ice thickness.

Ocean heat transport does not occur because the slab mixed layer ocean contains no circulation. Since ocean heat transport plays a significant role in the present-day geographical distribution of surface temperature, heat fluxes mimicking it must be imposed at the bottom of the mixed layer to maintain a realistic climate state. These fluxes vary geographically and seasonally and are determined prior to the model integration.

To isolate the simulated impact of water vapor feedback on the amplitude of the seasonal cycle, we integrate the model in two configurations: in the first ('control'), the model is run as it was was originally designed, with humidity values predicted by the hydrologic component transmitted to the portion of the model that calculates longwave radiation. In the second ('FWV'), water vapor is fixed at all grid points and all vertical levels to annual-mean values for the purposes of the calculation of longwave radiative transfer, though water vapor still undergoes seasonal and internal variations in the model's hydrologic component. In the FWV configuration, the effect of the seasonal variation of humidity on the atmosphere's greenhouse effect is removed, eliminating the contribution of water vapor feedback to the annual cycle of temperature. The annual-mean humidity field prescribed in the longwave radiative transfer component of the FWV model was calculated from the climatology of the control model. Both model configurations were integrated for 20 years to provide a statistically stable climatology. Of course water vapor also absorbs solar

radiation, so it is likely that the seasonal cycle of water vapor depicted in fig 1 would also reduce radiative damping of the SAT seasonal cycle through its influence on the solar radiation budget. This effect is not included in our experimental framework. However, it is probably quite small; Ramanathan and Coakley (1978) showed that the impact of the shortwave component of water vapor feedback in the context of climate change is approximately an order of magnitude smaller than the longwave component.

Prescribing water vapor to annual-mean values in the FWV model's longwave radiative transfer subroutine results in a systematic radiative imbalance that persists throughout the calendar year. If this radiative imbalance were not compensated for, the FWV model would drift toward a different mean state from the control model. To prevent this, the heat fluxes mimicking the heat transport within the ocean were adjusted to force the FWV model to maintain a realistic mean state. This additional adjustment has no seasonal variation, ensuring that it does not contribute in any way to the differences in the behavior of the two models' seasonal cycles.

3 Heuristic Model for SAT Response to Seasonal Forcing

We develop here a heuristic model for the SAT response to the seasonal cycle of incoming insolation. This simple model will aid in understanding the simulated and observed amplitude and phase of the seasonal cycle of extratropical SAT, as well as diagnosing the effect of climate feedbacks such as water vapor feedback on the seasonal cycle. The heuristic model has four elements designed to take into account the essential processes controlling the amplitude and phase of the seasonal cycle:

(1) **Forcing.** As noted in section 1, the focus of this paper is on the seasonal cycle in NH and SH extratropical regions bounded by 23.5° latitude. The solar forcing averaged over the both

NH and SH regions is well-approximated as a sine wave with a period of one year (fig 2). This then is how we incorporate it into the heuristic model.

(2) **Heat Storage.** Because the atmosphere and the ocean have a finite heat capacity, they can store some of the anomalous heat associated with the seasonally-varying solar forcing. We represent this effect as a temperature tendency multiplied by a heat capacity.

(3) **Radiative Damping.** The most obvious source of damping of the seasonal temperature anomaly is outgoing longwave radiation at the top of the atmosphere. When the temperature increases (decreases) this flux also increases (decreases). Water vapor feedback may reduce this damping by trapping more (less) infrared radiation during warm (cold) months. The seasonal cycle of reflected solar radiation at the top of the atmosphere likely also reduces the net radiative damping, since the earth's surface is less (more) reflective of sunshine during the warm (cold) months. The seasonal cycle of cloudiness may either attenuate or strengthen the radiative damping through its impact on outgoing longwave and reflected solar radiation. For the sake of simplicity, we represent the total radiative damping in the heuristic model with a damping term proportional to the SAT anomaly.

(4) **Lateral Damping.** The energy budget of the extratropical region is governed not only by net radiation at the top of the atmosphere and heat storage within it, but also by heat exchange with tropical regions equatorward of 23.5°. We include a term designed to mimick this lateral heat transport in the heuristic model. Since tropical temperatures vary much less on seasonal time scales than temperatures in mid to high latitudes (see fig 7), the seasonal variation in the thermal contrast between the extratropics and the tropics is governed largely by the magnitude of the seasonal mid to high latitude temperature anomaly. If the heat transport across 23.5° into the tropical zone is roughly proportional to this thermal contrast, becoming greater than average

during summertime, and less than average during wintertime, we can incorporate it in the heuristic model as a linear damping process. In section 7 we evaluate the validity of the assumption of linear damping.

Here then are the four terms noted above expressed in mathematical form:

$$C\frac{\partial T'}{\partial t} = -(\lambda_R + \lambda_L) \cdot T' + \frac{Q_o}{2} sin(\frac{2\pi}{\tau_f} t) \tag{1}$$

where C is the effective heat capacity of the system, T' is the SAT departure from annual mean conditions, Q_o is the amplitude of the seasonal cycle of sunshine, τ_f is the time scale of the forcing (in this case, one year), λ_R is the coefficient associated with radiative damping of the SAT anomaly, and λ_L is the coefficient associated with lateral damping of the SAT anomaly.

Letting $\lambda = \lambda_R + \lambda_L$, and defining a characteristic response time scale $\tau_r = C/\lambda$ this differential equation is easily solved, and has the following solution for T':

$$T' = \frac{T'_o}{2} sin(\frac{2\pi}{\tau_f} t - \varphi) \tag{2}$$

where

$$tan\varphi = 2\pi \frac{\tau_r}{\tau_f} \tag{3}$$

and

$$T'_o = \frac{Q_o}{\lambda cos\varphi} \cdot \frac{\tau_r^{-2}}{\tau_r^{-2} + (\tau_f/2\pi)^{-2}} \tag{4}$$

The relative magnitudes of the forcing and response time scales are critical in determining the amplitude and phase of the response. In particular, if the response time scale is very short

compared to that of the forcing ($\tau_r \ll \tau_f$), then the system will be in equilibrium and in phase with the forcing, and the magnitude of the response will be governed by the damping (λ):

$$T_o' = \frac{Q_o}{\lambda} \tag{5}$$

In the other extreme, if the response time scale is very long compared to that of the forcing ($\tau_r \gg \tau_f$), then the system's response will lag the forcing by 90° and its magnitude will be controlled by the heat capacity:

$$T_o' = \frac{Q_o}{C} \cdot \frac{\tau_f}{2\pi} \tag{6}$$

In between these two extremes, both the heat capacity and the damping influence the magnitude and phase of the system's response. The seasonal cycle of extratropical SAT is generally a little over one month out of phase with the seasonal cycle of sunshine, and so is somewhere between these two extremes. The fact that the amplitude and phase of the seasonal cycle is controlled by both heat capacity and damping effects is one reason it is difficult to predict how climate feedbacks such as water vapor feedback might affect the seasonal cycle.

4 Effect of Water Vapor Feedback on SAT Amplitude and Phase

Before describing how water vapor feedback affects the amplitude and phase of the SAT seasonal cycle, we first confirm that the seasonal variation in humidity shown in fig 1 reduces the top-of-the-atmosphere radiative damping of SAT. Fig 3 demonstrates that when the seasonal variation in humidity is replaced by annual mean humidity values in the radiative transfer code of the FWV model, the radiative damping increases systematically at all latitudes poleward of 23.5°. In the FWV model, the radiative damping is on average 30-50% larger than in the control

model. This difference is reflected in the calculation of the aggregate radiative damping for the NH and SH extratropical regions, done for each hemisphere by regressing the net outgoing radiation against SAT averaged over the entire region. In the NH, this regression is 6.6 $\mathrm{Wm}^{-2\circ}\mathrm{C}^{-1}$ for the FWV model, while it is only 4.7 $\mathrm{Wm}^{-2\circ}\mathrm{C}^{-1}$ for the control model. In the SH, the radiative damping for the entire extratropical region is 14.8 $\mathrm{Wm}^{-2\circ}\mathrm{C}^{-1}$ in the FWV model, and 11.6 $\mathrm{Wm}^{-2\circ}\mathrm{C}^{-1}$ in the control model.

Readers may be interested to know why the radiative damping values are larger than those typically associated with radiative damping of SAT. For example, in the climate change context, the equilibrium global-mean response to a doubling of CO_2 is thought to lie in the 1.5 to 4.5°C range (Cubasch and Meehl, 2001). Assuming a radiative forcing of 4 Wm^{-2} for a doubling of CO_2, this translates into an range of values for SAT radiative damping of 1.1 to 2.7 $\mathrm{Wm}^{-2\circ}\mathrm{C}^{-1}$, well below the values seen at any latitude in fig 3. The radiative damping values are so much larger in the seasonal cycle context because of the large seasonal variation in the atmosphere's vertical temperature structure in both hemispheres. The creates a very strong lapse rate feedback: Since the extratropical atmosphere is more (less) stratified in winter (summer), outgoing longwave radiation at the top of the atmosphere decreases (increases) beyond what would be expected by the seasonal decrease (increase) in SAT alone. The anomaly in longwave radiative trapping warms (cools) the atmosphere, contributing heavily to the radiative damping of winter (summer) SATs.

If SAT were in equilibrium with solar forcing on seasonal time scales and there were no transfer of heat across 23.5° latitude, we could predict the relative amplitudes of the SAT seasonal cycle averaged over the extratropics in the control and FWV models based on the ratio of the radiative damping in the two experiments. In the language of the heuristic model developed in section 3, the amplitude would be predicted by eq 5, so that the ratio of the seasonal

cycle amplitudes in the two experiments would be determined by the ratio of the values of the radiative damping. For example, in the NH, the radiative damping in the FWV experiment is 46% larger than in the control experiment, implying that the control/FWV ratio of the seasonal cycle amplitudes ought to be 1.46 if the system were in equilibrium with the forcing and there were no lateral damping. The analogous calculation for the SH implies a control/FWV amplitude ratio of 1.31. Examining the actual amplitudes of the SAT seasonal cycle averaged over the NH and SH extratropical regions in the two models (figs 4a and b), we see while the amplitudes are somewhat larger in the control model in both hemispheres, the effect is smaller than what one would expect based on the effect on radiative damping alone. In the NH, the control/FWV ratio of the amplitudes is 1.17, while in the SH it is 1.13. The effect of water vapor feedback on the phase of the seasonal cycle of SAT is also measurable but not large. From figs 4c and d, the SAT lags the solar forcing by about 30 days in both hemispheres in both models, with the lag being a few days less in the FWV model.

To understand why the simulated impact of water vapor feedback on the amplitude and phase of the seasonal cycle is relatively small, we examine the heat budget of NH and SH extratropical regions using the framework outlined in section 3. The top row of fig 5 shows the seasonal deviation of incoming solar radiation in the NH and SH regions (i.e. the forcing term of eq 1, $Q_o sin(\frac{2\pi}{\tau_f}t)$). The second row shows the seasonal cycle of outgoing longwave radiation and reflected solar radiation. This corresponds to the radiative damping of the seasonal temperature anomaly ($-\lambda_R \cdot T'$). The third row shows the seasonal deviation of the heat export out of NH and SH regions. This corresponds to the lateral damping term of eq 1 ($-\lambda_L \cdot T'$). The seasonal deviation of both the heat export and outgoing radiation components are roughly in phase with and approximately proportional to the seasonal cycle of SAT. This provides some validation of the linear damping term used to model these two phenomena in eq 1. The bottom row shows

the seasonal cycle of heat storage (analogous to $C\frac{\partial T'}{\partial t}$). The amplitude of the seasonal cycle of storage is larger in the SH because of the larger ocean area in the SH.

From fig 5, it is apparent that in both hemispheres, the seasonal cycle of the forcing is balanced by approximately equal contributions from heat storage, radiative damping, and lateral damping. The fact that heat storage cannot be neglected in the total heat budget confirms that the seasonal cycle of SAT is somewhat out of equilibrium with the forcing. This reduces somewhat the effect of damping mechanisms, including radiative and lateral damping effects, on the amplitude of the SAT seasonal cycle. This may be one reason why water vapor feedback has relatively little impact on the SAT seasonal cycle. In addition, in both hemispheres, the lateral damping is comparable in magnitude to the radiative damping. We have seen above that eliminating water vapor feedback increases the radiative damping by 30-50%, but this has a smaller relative effect on the total damping when both lateral and radiative damping are considered. Because SAT is not in equilibrium with the solar forcing, and because radiative and lateral effects compete to damp the annual cycle of SAT, the classical climate feedback mechanisms such as water vapor feedback have a significantly smaller impact on the amplitude or phase of the SAT seasonal cycle than would be expected based purely on an analysis of their effect on radiative damping. In the next section we make these observations more quantitative using the heuristic model developed in section 3.

5 Primary Controls on SAT Amplitude and Phase

5.1 Consistency Check on the Heuristic Model

The information presented in figs 4c and d and 5 allows for a check of the predictive power of the heuristic model. In this section, we see if the model can predict the correct amplitude of the SAT

seasonal cycle given information about the phase of the seasonal cycle and the damping of the seasonal anomaly of SAT. The method is as follows: Using information about the phase of SAT (grey bars in figs 4c and d), we can use eq 3 to calculate the characteristic response time scale of the system, τ_r. We can also calculate λ by regressing the radiative and lateral fluxes shown in figs 5c-f against SAT. Given Q_o, we can then use eq 4 to predict the amplitude of the SAT seasonal cycle. Since $\tau_r = C/\lambda$, we can also use our knowledge of λ to solve for the effective heat capacity, C.

Table 1 shows the results of this exercise for the control model. In both hemispheres, the heuristic model does a reasonable job of predicting T_o', though the predicted values tend to be somewhat too large. The heuristic model also succeeds quite well in predicting the relative amplitudes of the SAT seasonal cycle in the two hemispheres. For example, the predicted amplitudes are 2.3 times larger in the NH than the SH, while the simulated amplitudes are 2.5 times larger in the NH.

The heuristic model can also be used to predict with surprising accuracy the relatively small change in the amplitude of the seasonal cycle when water vapor feedback is removed. In analogy to fig 5, the seasonal cycle of the various components of the heat budget can be calculated for the FWV model (not shown), providing a means to calculate λ for the FWV model. This, together with the phase information contained in the white bars of figs 4c and d can be used to predict T_o'. The results are shown in table 2. Once again the heuristic model overestimates T_o' somewhat in both hemispheres. However, it does an excellent job predicting the relative effect of water vapor feedback on seasonal cycle amplitude. Both the predicted and simulated ratio (control/FWV) of the NH seasonal cycle amplitude is 1.17. In the SH the predicted and simulated ratios differ only slightly, with the heuristic model predicting an 11% enhancement of seasonal cycle amplitude resulting from the additional damping due to the removal of water vapor feedback, while the

	Q_o	**lag**	τ_r	λ_R	λ_L	λ	**C**	T_o' **(predicted)**	T_o' **(simulated)**
NH	354.0	33.2	37.3	4.7	5.1	9.7	12.6	30.6	26.2
SH	393.6	31.3	34.7	11.6	14.3	25.8	23.0	13.1	10.3

Table 1: The heuristic model's predictions of the amplitude of the SAT seasonal cycle and effective heat capacity given the lag and total damping (control model). Column 1: The amplitude of the solar forcing (Wm^{-2}). Column 2: The lag (days) of the SAT seasonal cycle behind the solar forcing (same as grey bars of figs 4c and d). Column 3: The characteristic response time scale (days) of the extratropical region calculated from the lag shown in column 2. Column 4: The radiative damping (Wm$^{-2\circ}$C^{-1}) of the seasonal SAT anomaly (i.e. the regressions of the fluxes shown in figs 5c and d against SAT). Column 5: The lateral damping (Wm$^{-2\circ}$C^{-1}) of the seasonal SAT anomaly (i.e. the regressions of the fluxes shown in figs 5e and f against SAT). Column 6: The total damping ($\lambda_L + \lambda_R$). Column 7: The effective heat capacity, given in terms of the depth (m) of water in the open ocean within the extratropical region that, when added to the atmosphere's heat capacity, provides the correct response time scale τ_r given λ. Open ocean is defined as the ocean area where no sea ice is simulated at any point in the calendar year. The area of open ocean is of course different in the two hemispheres, being much larger in the SH than the the NH. Column 8: Amplitude of the control SAT seasonal cycle predicted by the heuristic model ($^\circ$C). Column 9: Amplitude of the SAT seasonal cycle simulated by the control model ($^\circ C$).

	Q_o	**lag**	τ_r	λ_R	λ_L	λ	**C**	T_o' **(predicted)**	T_o' **(simulated)**
NH	354.0	29.1	31.9	6.6	5.3	11.9	13.4	26.1	22.3
SH	393.6	28.7	31.3	14.8	14.6	29.4	23.7	11.8	9.1

Table 2: As in table 1, except for the FWV model.

simulated enhancement is 13%.

The fact that the heuristic model's predictions are reasonably consistent with the actual behavior of the control and FWV models implies that it incorporates the most essential mechanisms controlling the amplitude and phase of the SAT seasonal cycle. Its predictions of the absolute magnitudes of the simulated SAT seasonal cycle tend to be somewhat too large, but it does an excellent job predicting the relative amplitudes between the NH and SH, as well as the impact of the removal of water vapor feedback.

One point of curiosity about the values presented in tables 1 and 2 are the values for C, the effective heat capacity of the atmosphere-ocean system (7th column). These values are given in terms of the depth of open ocean water within the extratropical region that, when added to the atmosphere's heat capacity, provides the correct response time scale, τ_r. They are substantially less than both the model's mixed layer depth of 50 m and the average depth of the observed seasonal thermocline, calculated by Manabe and Stouffer (1980) to be approximately 68 m. The discrepancy is easily reconciled by considering the fact that the values presented in tables 1 and 2 represent the effective amount of ocean needed to be perfectly in equilibrium and in phase with the seasonal cycle of SAT to provide the correct SAT phase lag. This will clearly be less than the total depth of the mixed layer, since the entire mixed layer from the surface down to the seasonal thermocline is not perfectly in equilibrium with overlying seasonal SAT variations. This is particularly true in ocean regions where local SAT is significantly influenced by air flowing from neighboring continents, such as over the western sides of the North Atlantic and North Pacific basins. The idea that the influence of large continents significantly reduces the effective degree of equilibrium of the ocean mixed layer with overlying SAT on seasonal time scales is also supported by a comparison of the values of C in the NH and SH. The effective depth of ocean water needed to provide the correct response time scale in the SH is almost twice as large as in

the NH, even after taking into account the larger ocean area in the SH. This is likely because the SH extratropical region has only about one-third as much land as its NH counterpart.

5.2 Predictions of the Heuristic Model

Because the heuristic model includes the essential mechanisms controlling the SAT response to seasonal forcing, we use it here to answer fundamental questions about how those mechanisms influence mid to high latitude seasonal cycle amplitude and phase.

Degree of equilibrium with the solar forcing. One interesting question is to what degree the SAT seasonal cycle is in equilibrium with the solar forcing. The SAT seasonal cycle in both hemispheres lags the solar forcing only by about 30 days, much less than the 90 or so days the lag would be if SAT were completely out of equilibrium with the solar forcing. This is consistent with the characteristic response time scales (τ_r) shown in table 2, which are short compared to the one-year time scale of the forcing. One way to illustrate how close close the SAT seasonal cycle is to equilibrium is to plug our values of Q_o and λ into eq 5 to predict a theoretical amplitude of the seasonal cycle if SAT were perfectly in equilibrium with the solar forcing. For the control case in the NH, this value is 36.5°C, less than 20% larger than the predicted amplitude of table 1 (where the fact that SAT is not perfectly in equilibrium is taken into account). For the SH control case, the predicted amplitude if SAT were in equilibrium is 15.3°C, also less than 20% larger than the predicted amplitude of table 1. In both hemispheres, SAT is surprisingly close to equilibrium with the solar forcing, with the radiative and lateral damping being the primary controls on its seasonal amplitude, rather than the effective heat capacity of the extratropical region. So the reason the amplitude of the SAT seasonal cycle is so small in the SH compared to the NH is not only the fact that the effective heat capacity is so much larger in this hemisphere, due to the predominance of ocean rather than land, as one might expect.

Rather, it is also the very large radiative and lateral damping of the seasonal cycle of SAT in the SH. For example, if we use the heuristic model to predict the SH seasonal cycle amplitude using the NH value of the total damping (λ), T_o' rises to 21.6°C, about 65% larger than the predicted amplitude shown in table 1, and nearly comparable to the predicted amplitude of T_o' for NH.

Importance of lateral damping. The heuristic model may also be used to highlight the importance of lateral damping in determining seasonal cycle amplitude and phase. That lateral damping is important is apparent from the fact that the lateral damping values in table 1 are larger than their radiative damping counterparts in both hemispheres. We can use the heuristic model to calculate the seasonal cycle amplitude if there were no seasonal heat exchange between the extratropics and tropics and the extratropical SAT seasonal cycle were damped purely by radiative processes. We merely replace the value of λ with the value of λ_R. In the NH, this would increase the value of T_o' to 45.4°C (about 50% larger than the predicted value of T_o' in table 1, and increase the lag of SAT behind the seasonal forcing from 33 to 54 days, nearly two months out of phase with the insolation. Similarly, in the SH, T_o' would rise to 20.4°C, more than 50% greater than the predicted value of T_o' in table 1, with the lag increasing from 31 to 54 days. Heat exchange across 23.5° latitude therefore reduces substantially both the amplitude and lag of the SAT seasonal cycle in mid to high latitudes.

6 Local Variations in the SAT Seasonal Cycle

In sections 4 and 5, we examined the seasonal cycle of SAT from the perspective of NH and SH regions bounded by 23.5° latitude. This proved to be a useful way of identifying the most important large-scale controls on the gross characteristics of the extratropical SAT seasonal cycle. In particular, we learned that heat transport across 23.5° is a damping process competitive

with radiative damping in determining the overall amplitude and phase lag of the seasonal cycle. In this section, we seek a more detailed and nuanced view of the seasonal cycle by examining the local variations in SAT amplitude and phase.

Fig 6 shows the local variations in the amplitude of the SAT seasonal cycle in the NH and SH for the control model and the NCEP re-analysis. The NCEP re-analysis, of course, is the result of observations having been assimilated into a numerical model of the atmosphere. The assimilation model applies an adjustment to these observations if they are inconsistent with the model's physics. Moreover, in areas where observations are missing altogether, the assimilation model simply fills in these gaps with simulated data. In the NH and in the SH equatorward of 45°S, observations are relatively plentiful, and the NCEP re-analysis data in these regions can be thought of as observations that have been checked for physical consistency. In the high latitudes of the SH, however, observations are very sparse, and the NCEP re-analysis data in these regions is probably best thought of as reflecting mostly the dynamics of the assimilation model.

The most striking feature of all panels of fig 6 is the much larger amplitude over land than ocean. The framework of the heuristic model developed in section 3 for the whole extratropical region can be applied to the local SAT response to seasonal forcing as well: Because the effective heat capacity of the land surface is so small compared to that of the ocean, SAT over land is in equilibrium with the solar forcing to a greater degree than SAT over the ocean and therefore attains a larger magnitude. Or, in the language of the heuristic model, C is smaller over land than ocean, reducing the response time scale, τ_T. The SAT response over land is therefore closer to the extreme embodied by eq 5 than it is over the ocean.

Evidence for the land and ocean having different response time scales to the seasonal forcing may also be found in the land-sea contrast in the lag of the seasonal cycle of SAT behind

the solar forcing. For example, this lag averaged over all land points poleward of 23.5° including both hemispheres is 22.2 days in the NCEP reanalysis, while over the ocean it is 51.1 days (see the caption of fig 4 for details on how the phase lag was calculated). Values for the simulated phase lag exhibit a comparable difference between land and ocean: Over land points, the lag behind the seasonal cycle of insolation is 24.7 days on average, while over ocean points it is 42.0 days.

The fact there there is measurable land-sea contrast in both the amplitude and phase of the seasonal cycle of SAT implies that horizontal heat transports within the extratropics are not effective enough to homogenize the SAT response to the seasonal cycle of insolation completely. However, we know from section 5 that lateral heat transport across 23.5° plays a very important role in determining the amplitude and phase of the SAT seasonal cycle, a fact which makes it highly likely that lateral heat exchange within the extratropics also exerts considerable control on local SAT amplitude and phase. Evidence of significant lateral heat exchange is apparent in fig 6. For example, in the NH in both model and the NCEP re-analysis (figs 6a and c), the seasonal cycle amplitude tends to be larger on the eastern side of the land masses. This is particularly apparent in Eurasia, where a steady increase in the amplitude of the seasonal cycle is visible going from west to east, until values in excess of 50°C are seen over Siberia. At the same time, over the NH oceans the largest amplitudes are seen on the western side of the Pacific and Atlantic basins.

This pattern is consistent with the predominantly westerly air flow in midlatitudes. In NH wintertime for example, the surface temperature of the Eurasian land mass becomes relatively low due to its small heat capacity. So an air parcel beginning at the eastern margin of the Atlantic—relatively warm through contact with the ocean surface—cools as it makes its way eastward across the landmass, releasing some of the heat it acquired over the Atlantic to the

cold land surface. The air parcel's progressive heat loss also means it has less and less energy to warm the surface, so that land surfaces further to the east tend to be exposed to colder air on average. This makes surface temperatures colder going east as well. Opposite reasoning applies during summertime, when Eurasia is on average warmer than the oceans at the same latitude. SATs over the eastern half of Eurasia are the least influenced of any location by the relative warmth (coldness) of the oceans during winter (summer).

The sheer size of the Eurasian continent is clearly the reason seasonal cycle amplitudes become so large there. Because other continents are smaller, air parcels traveling across them are not exposed to the land surface as long, limiting the progressive cooling (heating) of air parcels as they make their way across the land during winter (summer). For example, the amplitudes over North America, though relatively large, are typically about two-thirds as large as those over Eurasia. The effect is even more apparent in the SH (figs 6b and d). Here the difference between summer and winter temperatures over the midlatitude land masses in both the control modela and the NCEP re-analysis is only about 10-20°C, less than half of the typical values seen than over land in the NH.

Although the geographical distribution of the SAT seasonal cycle amplitude is broadly similar in the control model and the NCEP re-analysis in the NH, there are notable differences between the two data sets. For example, comparing figs 6a and c, it is apparent that over Siberia the control seasonal cycle amplitude is larger than that of the NCEP re-analysis. This is likely because the control model computes surface temperature over land as a simple balance among sensible heat, latent heat, and radiative fluxes without taking into account any heat storage within the land surface. This gives the model an unrealistically small effective heat capacity over land.

The simulated SH seasonal cycle amplitude is also broadly similar to the NCEP re-analysis (figs 6b and d), though over the Antarctic continent the amplitudes in the NCEP re-analysis are

significantly larger than those of the control model. As noted above, the high latitude SH NCEP re-analysis data probably is mainly a reflection of the dynamics contained in the NCEP assimilation model, so that the comparison in Antarctica is mostly a comparison of the control and NCEP assimilation model simulations. The control model does not have a stability dependent boundary layer parameterization; it simply diffuses heat upward in the lowest few kilometers of the atmosphere to mimick the turbulent redistribution of heat within the boundary layer regardless of the background stratification. In the highly stratified SH polar atmosphere, this likely results in excessive upward diffusion of heat from the surface, unrealistically increasing the effective heat capacity of the control model's lowest layer and attenuating the amplitude of the seasonal cycle. The stability-dependent boundary layer parameterization employed in the NCEP assimilation model means that comparatively little heat is diffused upward in the highly stratified polar atmosphere. This guarantees a smaller effective heat capacity than the control model for the lowest layer, and therefore a larger seasonal cycle amplitude.

7 Conclusion

By comparing the seasonal cycle of SAT in an atmosphere-mixed layer model where the large seasonal variation in humidity is allowed to affect longwave radiation to one where it is not, we examine the impact of water vapor feedback on seasonal cycle amplitude and phase. Water vapor feedback is thought to be the most powerful positive feedback to climate variations. However, it has a surprisingly small amplifying effect of about 10-20% on the amplitude of the seasonal cycle. Its effect on phase is also small. This is mainly because the extratropical seasonal cycle is damped not only by radiative processes, but also by heat exchange between the extratropics and tropics. When temperatures are cold (warm) during winter (summer), an anomalously large (small) amount of heat is transported from the tropics into the extratropics. On a Wm^{-2} basis, this

damping mechanism is slightly more effective than radiative damping, substantially diluting the effects of the classical radiative climate feedbacks such as water vapor feedback. Because the seasonal cycle is so effectively damped by both radiative fluxes and horizontal heat exchange, it is in equilibrium with the solar forcing to a surprisingly large degree, with a much smaller amplitude than would be expected if radiative feedbacks alone were responsible for the damping. We show that if there were no lateral damping, the amplitude of the extratropical SAT seasonal cycle would increase by approximately 50% in both hemispheres, while its lag behind the solar forcing would increase from one to about two months.

Classical radiative feedbacks other than water vapor feedback probably also influence the radiative damping of the SAT seasonal cycle. For example, the large seasonal variation of snow and sea ice (e.g. Robock 1980) likely reduces the radiative damping of the SAT seasonal cycle through its effect on surface albedo. A larger cryosphere in winter increases the proportion of sunlight reflected to space, reducing wintertime temperatures further, while the smaller summertime cryosphere reduces the planetary albedo, increasing summertime temperatures. However, since lateral damping is slightly stronger than all radiative feedbacks combined, it seems likely that surface albedo feedback, like water vapor feedback, has a relatively small impact on seasonal cycle amplitude and phase.

In spite of their importance in determining the overall amplitude and phase of the seasonal cycle, large-scale heat transports do not succeed in homogenizing completely the local characteristics of the seasonal cycle in extratropics, as demonstrated by an detailed examination of the seasonal cycle amplitude and phase in the model and the NCEP re-analysis. In both hemispheres in both model and observations, the seasonal cycle has a larger amplitude over land than ocean, with the amplitude over a continent corresponding directly with the continent's size. The seasonal cycle is also out of phase with the solar forcing to a greater degree over ocean

than over land in both model and observations.

Our conclusion that climate radiative feedbacks thought to be important for climate change make only a small contribution to the amplitude of the SAT seasonal cycle provides an explanation for some of the results seen in Covey et al. (2000). These authors found only a weak correlation between equilibrium climate sensitivity to a CO_2 doubling and seasonal cycle amplitude, with equilibrium climate sensitivity accounting for approximately 15% of the variance in seasonal cycle amplitude. Since equilibrium climate sensitivity is determined almost exclusively by classical climate radiative feedbacks, it ought to be a poor predictor of seasonal cycle amplitude given that seasonal cycle amplitude is damped by horizontal heat transport as well as radiative processes. Moreover, certain radiative damping processes may behave differently in the seasonal cycle and climate change contexts. As noted in section 4, the longwave radiative damping is increased by a large seasonal cycle in the atmospheric lapse rate which has no identified analog in the climate change case. This would complicate the relationship between seasonal cycle amplitude and equilibrium climate sensitivity even if lateral heat transport played no role in the damping of the seasonal cycle.

In spite of the fact that water vapor feedback has little effect on seasonal cycle amplitude and phase, it still seems significant that the feedback itself operates in a similar way to the simple water vapor feedback hypothesized to play an important role in equilibrium climate sensitivity. The tight relationships between water vapor and temperature on seasonal time scales shown in fig 1 reflect the fact that relative humidity averaged over mid to high latitudes varies little throughout the year in both model and observations (not shown). This is exactly how water vapor feedback behaves in nearly all climate models; as temperatures increase as a result of an increase in greenhouse gases, water vapor increases in the atmosphere so that relative humidity remains approximately constant. Surface albedo feedback is also positive in the context of the

seasonal cycle, as noted above, though some investigation is necessary to determine whether the surface albedo/temperature relationship in the seasonal cycle context is similar to the surface albedo/temperature relationship in the climate change context.

The importance of heat exchange across 23.5° latitude highlights the stabilizing role of the tropics in the extratropical seasonal cycle. Fig 7 shows the climatological SAT seasonal cycle simulated by the control model in NH and SH extratropical regions and the tropics. The near constancy of the climatological tropical climate throughout the year provides an anchor that strongly limits the response of extratropical climate to the seasonal variation of solar radiation in both hemispheres. This, coupled with the large radiative damping of the extratropical seasonal cycle, is the main reason the extratropical climate is so surprisingly insensitive to the huge seasonal solar forcing; the values for the total damping given in tables 1 and 2 are on the order of tens of $\mathrm{Wm}^{-2\circ}\mathrm{C}^{-1}$ in both hemispheres, about an order of magnitude larger than the range of damping values thought to control the equilibrium climate response to a doubling of CO_2.

Acknowledgments.

Alex Hall is supported by an NSF CAREER award ATM–0135136. The authors wish to thank James McWilliams and David Neelin for stimulating discussions on this topic.

References

Broccoli, A.J., 2000: Tropical cooling at the last glacial maximum: an atmosphere-mixed layer ocean model simulation. *J. Clim.*, **13,** 951-976.

Cess, R.D. and Coauthors, 1991: Interpretation of snow-climate feedback as produced by 17 general circulation models. *Science*, **253,** 888-891.

Cess, R.D. and Coauthors, 1996: Cloud feedback in atmospheric general circulation models: An update. *J. Geophys. Res.*, **101,** 12791-12794.

Covey, C. and Coauthors, 2000: The seasonal cycle in coupled ocean-atmosphere general circulation models. *Clim. Dyn.*, **16,** 775-787.

Cubasch, U., G.A. Meehl, and Coauthors, 2001: Projections of Future Climate Change, in *Climate Change 2001: The Scientific Basis*. Cambridge, UK: Cambridge University Press, pp 525-582.

DelGenio, A.D., W. Kovari, and M.S. Yao, 1994: Climatic implications of the seasonal variation of upper tropospheric water vapor *Geophys. Res. Lett.*, **21,** 2701-2704.

Gordon, C.T., and W.F. Stern, 1982: A description of the GFDL global spectral model. *Mon. Wea. Rev.*, **110,** 625-644.

Hall, A., 2003: Role of surface albedo feedback in climate. Part II: Externally-forced climate change. submitted to *J. Clim.*.

Hall, A., and S. Manabe, 1999: The Role of Water Vapor Feedback in Unperturbed Climate Variability and Global Warming. *J. Clim.*, **12,** 2327-2346.

Hartmann, D., and K. Larson, 2002: An important constraint on tropical cloud-climate feedback. *Geophys. Res. Lett.*, doi:10.1029/2002GL015835.

Held, I.M., and B.J. Soden, 2000: Water vapor feedback and global warming. *Ann. Rev. Energy Environ.*, **25,** 441-475.

Ingram, W.J., C.A. Wilson, and J.F.B. Mitchell, 1989: Modeling climate change: an assessment of sea ice and surface albedo feedbacks. *J. Geophys. Res.*, **94(D6),** 8609-8622.

Lindzen, R.S., M.D. Chou, A. Hou, 2001: Does the earth have an adaptive iris? *Bull. Am. Met. Soc.*, **82,** 417-432.

Manabe, S., 1969: Climate and the Ocean Circulation: I. The Atmospheric Circulation and the Hydrology of the Earth's Surface. *Mon. Wea. Rev.*, **97,** 739-774.

Manabe, S., R.J. Stouffer, 1980: Sensitivity of a Global Climate Model to an Increase of CO_2 Concentration in the Atmosphere. *J. Geophys. Res.*, **85(C1),** 5529-5554.

Manabe, S., R.T. Wetherald, 1980: On the horizontal distribution of climate change resulting from an increase in CO_2 content of the atmosphere. *J. Atmos. Sci.*, **37,** 99-118.

Mitchell, J.F.B., W.J. Ingram, 1992: Carbon dioxide and climate-mechanisms of changes in cloud. *J. Clim.*, **5,** 5-21.

Ramanathan, V., and J.A. Coakley, 1978: Climate modeling through radiative-convective models. *Rev. Geophys. Space Phys.*, **16,** 465-489.

Robock, A., 1980: The seasonal cycle of snow cover, sea ice and surface albedo. *Mon. Wea. Rev.*, **108,** 267-285.

Robock, A., 1983: Ice and snow feedbacks and the latitudinal and seasonal distribution of climate sensitivity. *J. Atmos. Sci.*, **40,** 986-997.

Wetherald, R.T., 1996: Feedback processes in the GFDL R30 - 14 level general circulation model. In *Climate Sensitivity to Radiative Perturbations: Physical Mechanisms and Their Validation*, NATO ASI Series I, Vol. 34, Berlin; Heidelberg: Springer-Verlag, 251-266.

Wetherald, R.T., and S. Manabe, 1988: Cloud feedback processes in a general circulation model. *J. Atmos. Sci.*, **45,** 1397-1415.

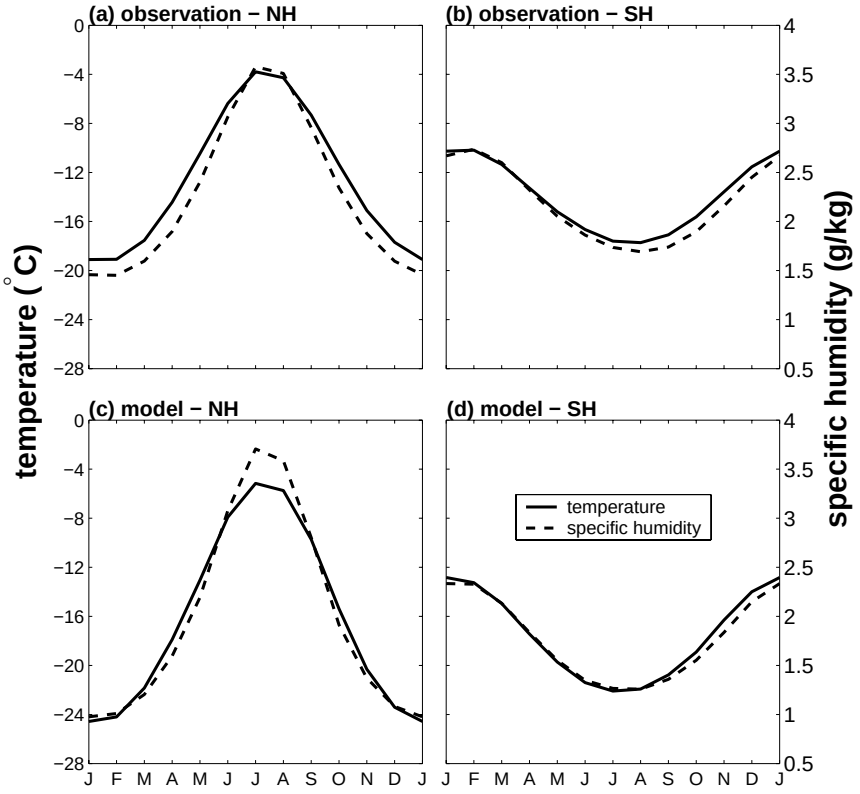

Figure 1: Seasonal cycle of lower to mid tropospheric mean temperature (solid lines) and specific humidity (dashed lines) averaged over the extratropics of the two hemispheres (bounded by 23.5° latitude): (a) NH observation (NCEP re-analysis). (b) SH observation. (c) NH control simulation. (d) SH control simulation. Lower to mid troposphere averages were calculated by pressure weighting the data from the surface to 300 hPa.

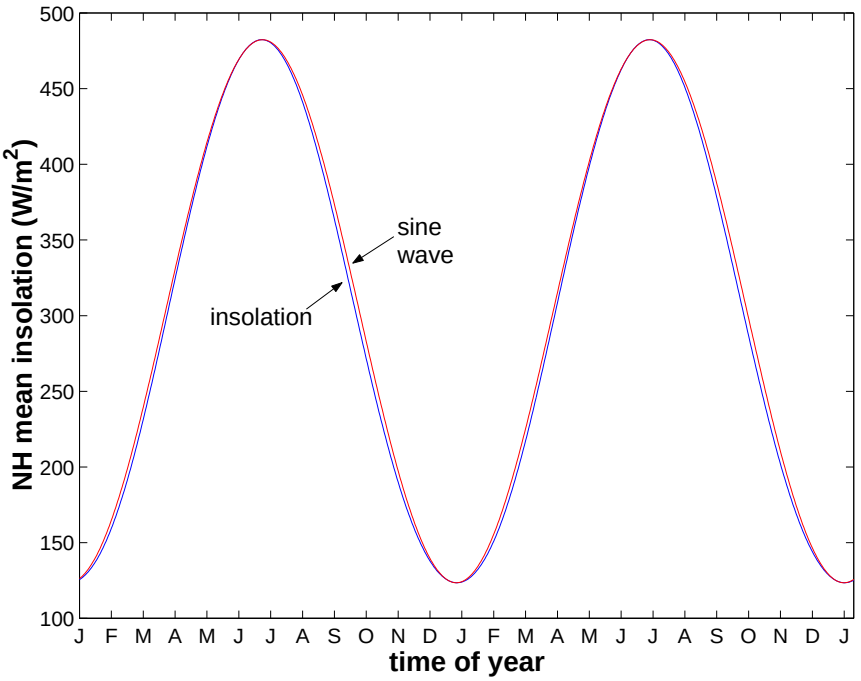

Figure 2: Seasonal cycle of area-weighted incoming solar insolation averaged over the NH poleward of 23.5° throughout the year. Comparison to a sine wave is also shown.

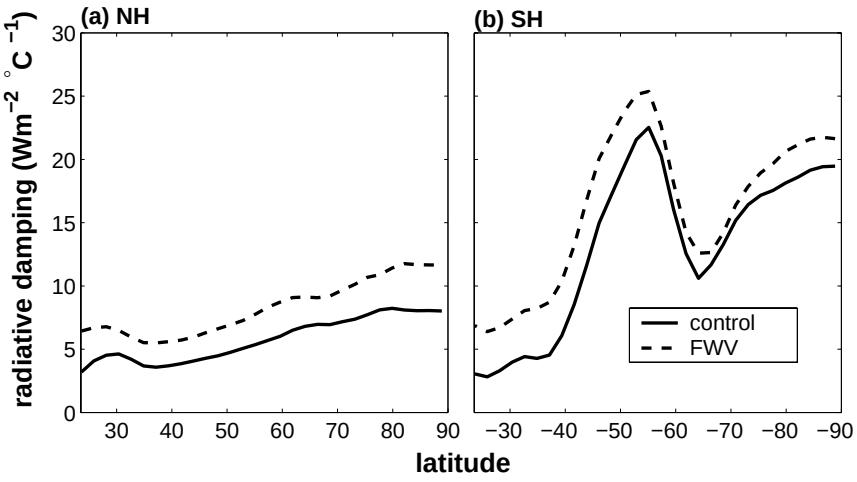

Figure 3: Zonal-mean radiative damping of the seasonal cycle of SAT poleward of 23.5° in the (a) NH and (b) SH. Values for the control model are shown with solid lines, while those of the FWV model are shown with dashed lines. Radiative damping was calculated by regressing climatological monthly-mean, zonal-mean net outgoing radiation (Wm^{-2}) against zonal-mean SAT ($^{\circ}$C). Net outgoing radiation is the sum of reflected solar radiation and outgoing longwave radiation.

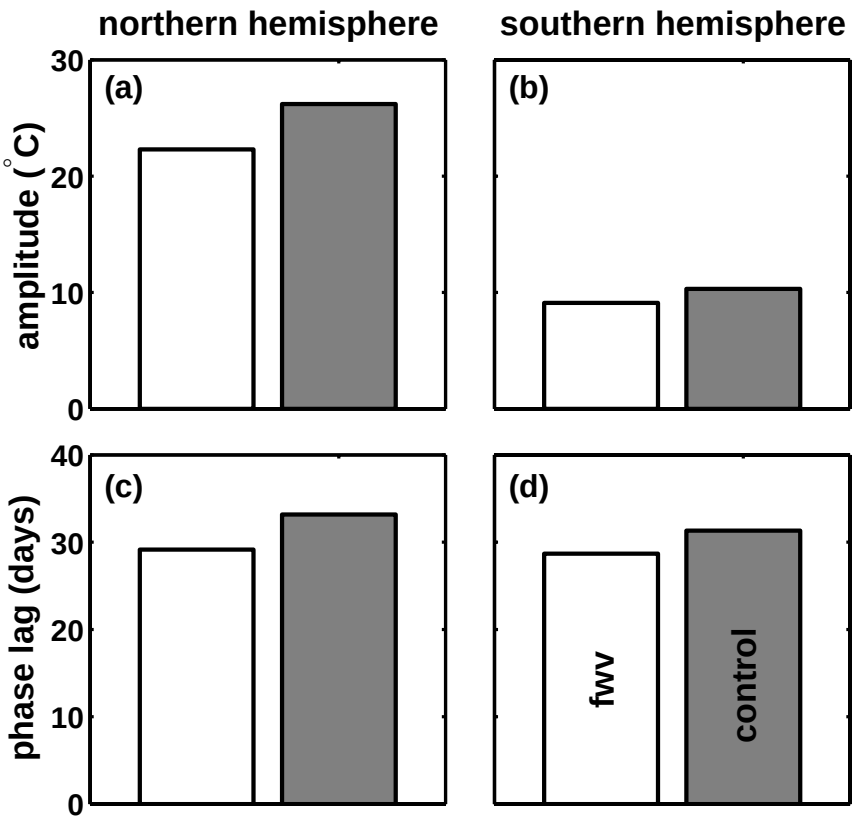

Figure 4: Amplitude of the seasonal cycle of SAT averaged over NH (panel a) and SH (panel b) extratropical regions bounded by 23.5° latitude. Lag averaged over NH (panel c) and SH (panel d) regions bounded by 23.5° latitude of the seasonal cycle of SAT relative to the solstices. This quantity is calculated by averaging the time lag of the temperature maximum behind the summer solstice and the time lag of the temperature minimum behind the winter solstice. In each panel, the left bar is for the FWV model, while the right bar (shaded grey) is for the control model.

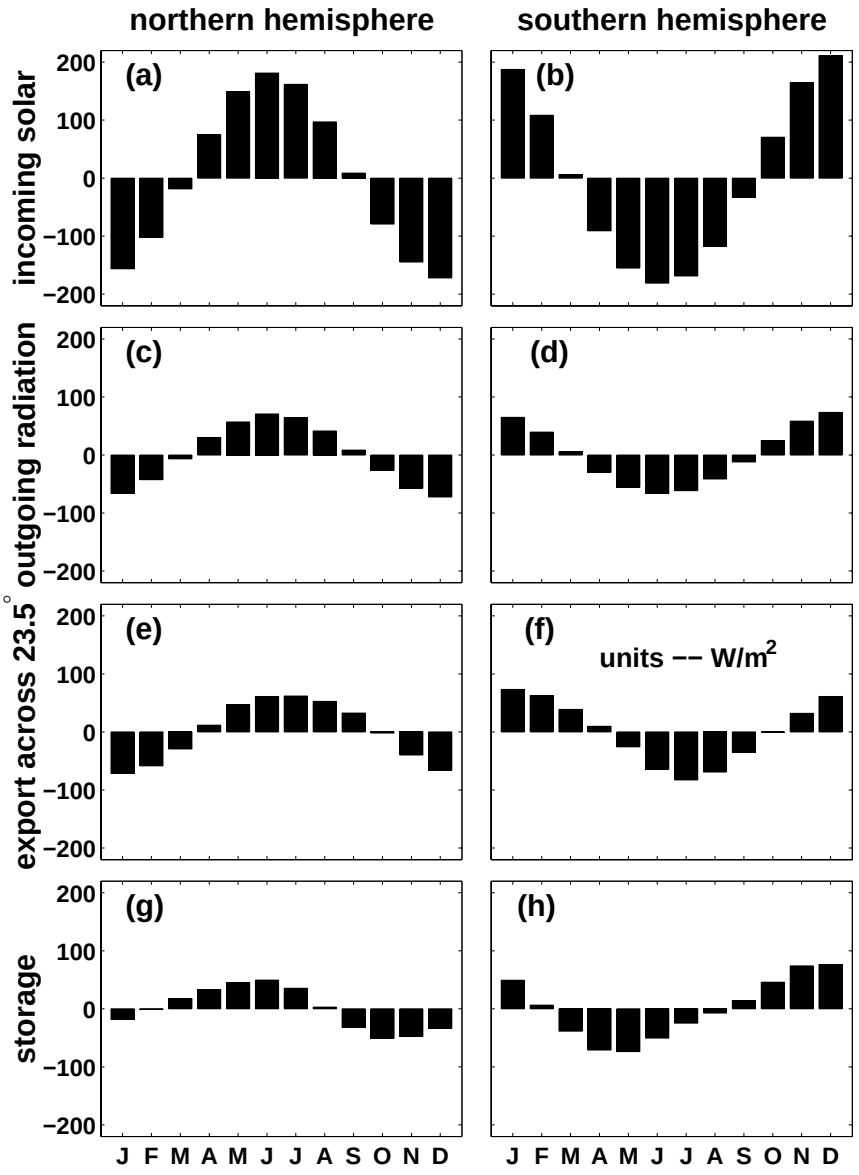

Figure 5: Seasonal deviation in the control simulation of the components of the heat budget of NH (1st column) and SH (2nd column) extratropical regions bounded by 23.5° latitude. Top row: incoming solar radiation at the top of the atmosphere. Second row: total outgoing radiation at the top of atmosphere (outgoing longwave + reflected SW). Third row: heat export from the extratropical region to the tropics, calculated as the residual of the components shown in the other rows. Bottom row: sum of the heat storage in the atmosphere and ocean. The atmospheric (oceanic) heat storage is calculated by multiplying the heat capacity of the atmosphere by the time rate of change of mean atmospheric (oceanic) temperature. The seasonal cycle of latent heat release associated with sea ice formation and melting is also included in the calculation of ocean heat storage. Units in all panels are Wm^{-2}.

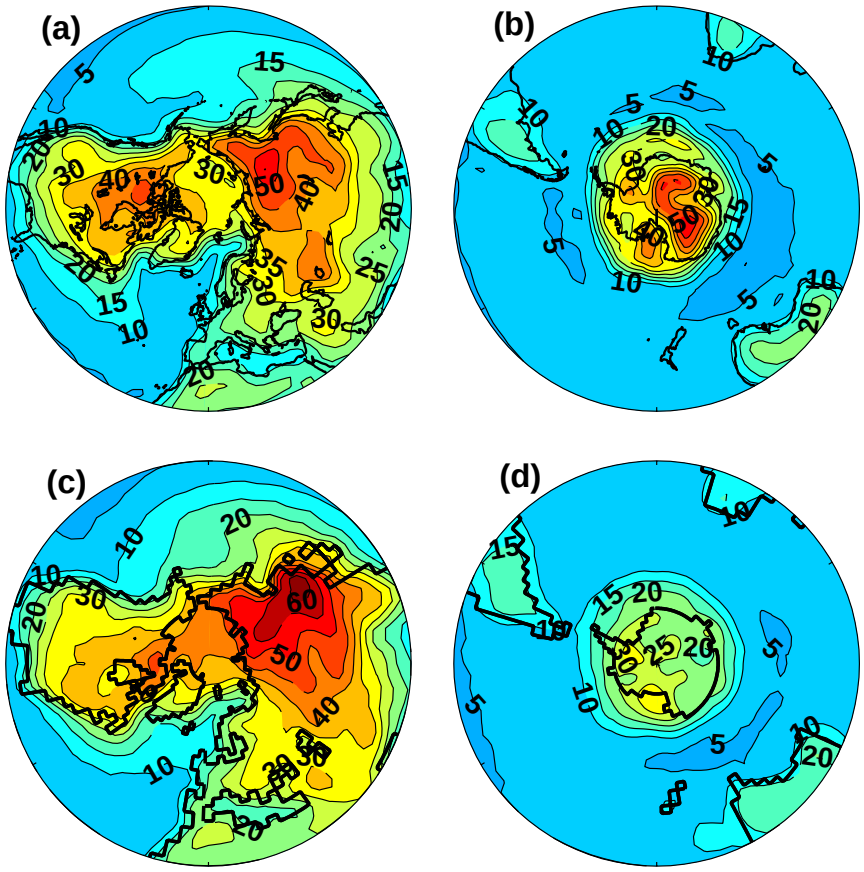

Figure 6: Geographical distribution of the amplitude of the seasonal cycle of SAT (°C) poleward of 23.5°. (a) NH observation (NCEP re-analysis). (b) SH observation. (c) NH control simulation. (d) SH control simulation. The amplitude of the seasonal cycle is defined at every location as the difference between the maximum and minimum temperatures occurring in a daily-mean composite seasonal cycle of SAT.

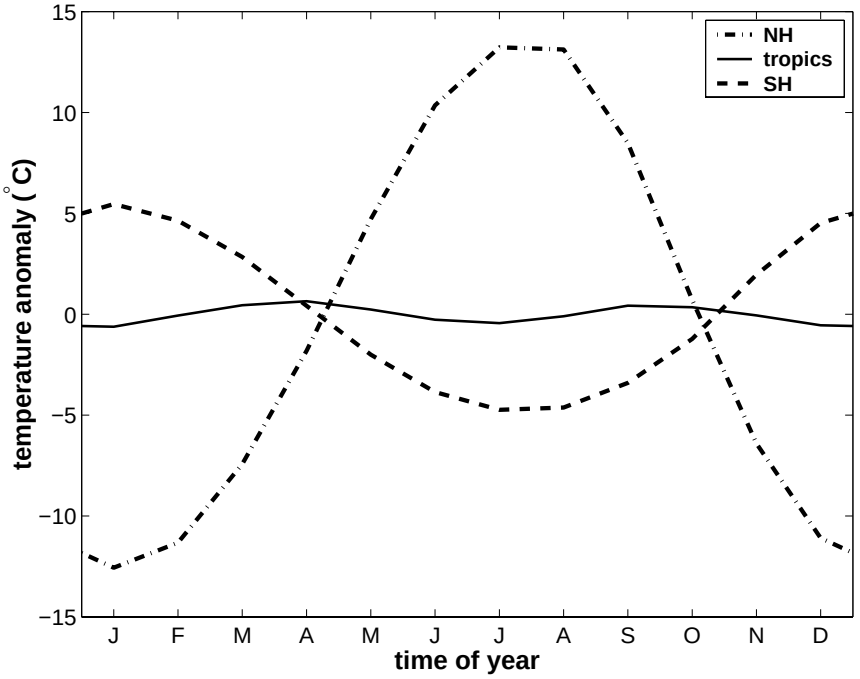

Figure 7: Simulated climatological seasonal cycle of SAT at monthly mean resolution in the control model averaged over three regions: NH extratropics bounded by 23.5°N, tropics bounded by 23.5°N and 23.5°S, and SH extratropics bounded by 23.5°S. The climatological seasonal cycle in the NCEP re-analysis calculated for the same regions looks nearly identical to this figure.